



## Research article

# Loco-regional staging of malignant pleural mesothelioma by integrated $^{18}\text{F}$ -FDG PET/MRI



D.J. Murphy<sup>a,b,\*,1</sup>, S.M. Mak<sup>c</sup>, A. Mallia<sup>a,b</sup>, S. Jeljeli<sup>a</sup>, J.J. Stirling<sup>a</sup>, V. Goh<sup>b,c</sup>, A. Bille<sup>d</sup>, G.J.R. Cook<sup>a,b</sup>

<sup>a</sup> King's College London & Guy's and St Thomas' PET Centre, London UK

<sup>b</sup> Department of Cancer Imaging, School of Biomedical Engineering and Imaging Sciences, King's College London, London UK

<sup>c</sup> Department of Radiology, Guy's and St Thomas' NHS Foundation Trust, London UK

<sup>d</sup> Department of Cardiothoracic Surgery, Guy's and St Thomas' NHS Foundation Trust, London UK

## ARTICLE INFO

## Keywords:

Mesothelioma

Staging

Neoplasm

Positron emission tomography computed tomography

Fluorodeoxyglucose F18

Magnetic resonance imaging

## ABSTRACT

**Aim:** To examine the performance of  $^{18}\text{F}$ -FDG PET/MRI in the loco-regional staging of malignant pleural mesothelioma (MPM).

**Methods:** Consecutive subjects with MPM undergoing pre-operative staging with  $^{18}\text{F}$ -FDG PET/CT who underwent a same day integrated  $^{18}\text{F}$ -FDG PET/MRI were prospectively studied. Clinical TNM staging (AJCC 7<sup>th</sup> edition) was performed separately and in consensus by two readers on the  $^{18}\text{F}$ -FDG PET/MRI studies, and compared with staging by  $^{18}\text{F}$ -FDG PET/CT, and with final pathological stage, determined by a combination of intra-operative and histological findings.

**Results:** 10 subjects (9 male, mean age 68 years) with biopsy-proven MPM (9 epithelioid tumours, 1 biphasic) were included. One subject underwent neo-adjuvant chemotherapy between imaging and surgery and was excluded from the clinical versus pathological stage analysis. Pathological staging was concordant with staging by  $^{18}\text{F}$ -FDG PET/MRI in 67% (n = 6) of subjects, and with  $^{18}\text{F}$ -FDG PET/CT staging in 33% (n = 3). Pathological T stage was concordant with  $^{18}\text{F}$ -FDG PET/MRI in 78% (n = 7), and with  $^{18}\text{F}$ -FDG PET/CT in 33% (n = 3) of subjects. Pathological N stage was concordant with both  $^{18}\text{F}$ -FDG PET/MRI and  $^{18}\text{F}$ -FDG PET/CT in 78% (n = 7) of cases. No subject had metastatic disease. There was good inter-observer agreement for overall PET/MRI staging (weighted kappa 0.63) with moderate inter-reader agreement for T staging (weighted kappa 0.59). All 6 subjects with prior talc pleurodesis demonstrated mismatch between elevated FDG uptake and restricted diffusion in areas of visible talc deposition.

**Conclusion:** Clinical MPM staging by  $^{18}\text{F}$ -FDG PET/MRI is feasible, and potentially provides more accurate loco-regional staging than PET/CT, particularly in T staging.

## 1. Introduction

Malignant pleural mesothelioma (MPM) is the most common primary malignant tumour of the pleura, arising from mesothelial cells [1]. Despite recent advances in tri-modality treatment (surgery, chemotherapy and radiotherapy), the prognosis remains dismal, with a five year survival of less than 10% [2].

Accurate staging is important to triage patients down the appropriate treatment pathway [3]. MPM has a complex morphology, with a rind-like appearance like that of the skin of an orange, growing across multiple imaging planes and crossing multiple tissue boundaries. The currently most widely used clinical staging system is the International Association for the Study of Lung Cancer (IASLC) and the International Mesothelioma Interest Group (IMIG) tumour, nodes and metastasis

**Abbreviations:** ADC, apparent diffusion coefficient; AJCC, American Joint Committee on Cancer; CT, computed tomography; DWI, diffusion-weighted imaging; FDG, 2-deoxy-2-[ $^{18}\text{F}$ ]fluoro-D-glucose; HASTE = half Fourier, acquired single shot turbo spin echo; IMIG, International Mesothelioma Interest Group; IASLC, International Association for the Study of Lung Cancer; IV, intravenous; MRI, magnetic resonance imaging; MPM, malignant pleural mesothelioma; MPR, multiplanar reformats; PET, positron emission tomography; ROI, region of interest; SD, standard deviation; SUV<sub>max</sub>, maximum standardised uptake value; TGV, total glycolytic volume; TNM, tumour, nodes and metastasis; VIBE, volume-interpolated breath-hold examination

\* Corresponding author at: Department of Radiology, St Vincent's University Hospital, Elm Park, Dublin 4, Ireland.

E-mail address: [david.murphy@st-vincent.ie](mailto:david.murphy@st-vincent.ie) (D.J. Murphy).

<sup>1</sup> Present address: Department of Radiology, St Vincent's University Hospital, Dublin, Ireland.

<https://doi.org/10.1016/j.ejrad.2019.04.003>

Received 6 November 2018; Received in revised form 4 March 2019; Accepted 4 April 2019

0720-048X/© 2019 Elsevier B.V. All rights reserved.

**Table 1**  
PET/MRI sequence parameters.

| Sequence                           | Region | Orientation | TR (ms) | TE (ms)   | Matrix size | Slice Thickness (mm) | FOV (mm)    | Voxel Size (mm)   |
|------------------------------------|--------|-------------|---------|-----------|-------------|----------------------|-------------|-------------------|
| T1-DIXON                           | WB     | Axial       | 4.02    | 1.23–2.46 | 175 × 320   | 5                    | 430 × 335.9 | 0.7i x 0.7i x 5   |
| T2 HASTE                           | WB     | Axial       | 700     | 107       | 175 × 320   | 5                    | 430 × 335.9 | 0.7i x 0.7i x 5   |
| DWI (b50, b900 s/mm <sup>2</sup> ) | WB     | Axial       | 8800    | 85        | 132 × 136   | 5                    | 430 × 417.4 | 1.6i x 1.6i x 5   |
| T1 DIXON + GAD                     | WB     | Axial       | 5.22    | 2.46–3.69 | 195 × 320   | 2                    | 380 × 308.8 | 0.6i x 0.6i x 2   |
| PET                                | WB     | Axial       | –       | –         | 172 × 172   | 2.03                 | 718 × 718   | 4.1 × 4.1 x 2.03r |

With interpolation (i) / reconstruction (r).

PET = positron emission tomography; MRI = magnetic resonance imaging; FOV = field of view; DWI = diffusion weighted imaging; GAD = intravenous gadolinium; WB = whole-body.

(TNM) system [4–6]. Due to the complex growth pattern in MPM, the current T stage descriptors rely on a qualitative, descriptive assessment of the extent of local tumour invasion. Qualitative assessment of tumour extension through local structures such as the diaphragm, pericardium and chest wall can be hard to perform accurately and reproducibly with CT [1,7,8].

MRI provides excellent soft tissue resolution, and is a potentially useful modality for MPM diagnosis and staging, but is not in widespread use [1]. The main strength of 2-deoxy-2-[<sup>18</sup>F]fluoro-D-glucose (FDG) positron emission tomography-computed tomography (PET/CT) in MPM clinical staging is in its ability to detect distal and occult metastases. Additionally, FDG PET provides functional information, such as metabolic activity or metabolic tumour volume, which may be prognostic [9,10]. However, it contributes little to local T staging above contrast enhanced CT [11].

Novel integrated PET/MRI systems have the potential to marry the superior soft tissue resolution and multi-parametric capabilities of MRI with the metabolic information provided by FDG PET in a single examination. A published series of six MPM patients by Schaarschmidt et al. has demonstrated that integrated PET/MRI is non-inferior to PET/CT in TNM staging of MPM [12]. Our hypothesis is that FDG PET/MRI is feasible in loco-regional staging of MPM, and may be superior to FDG PET/CT. The aim of our prospective study is to examine how integrated PET/MRI performs in loco-regional MPM staging, using pathological staging as the reference standard.

## 2. Materials & methods

### 2.1. Patients

This prospective study was approved by the institutional research ethics committee and all subjects gave informed consent. All pre-operative patients referred to the King's College London & Guy's and St Thomas' PET Centre (London, United Kingdom) for clinical FDG PET/CT staging for malignant pleural mesothelioma were considered for inclusion in this prospective single centre study. To fulfil inclusion criteria, subjects had to have a histological confirmed diagnosis of MPM, be potential operative candidates and have no contraindications to MRI. Ten patients (9 men, 1 woman, mean age of 68 ± 6.1 years with a range 51–73 years) and biopsy proven MPM consented to take part in the study. They had a single dose of radiotracer administered and underwent a same-day on-site FDG PET/MRI immediately following the clinical PET/CT scan. Final pathological TNM staging (7<sup>th</sup> edition) after surgical intervention was used as the gold standard for staging comparison.

### 2.2. <sup>18</sup>FDG PET/CT acquisition

<sup>18</sup>FDG PET/CT scans were all acquired in our institution using the same standard clinical protocol on one of two scanners (Discovery 710, GE Healthcare, Chicago, IL, USA). Patients were fasted for a minimum

of 6 h. A standard PET acquisition from skull base to upper thighs was acquired 60–90 minutes post-injection of 350 MBq (± 10%) of FDG. Image acquisition was performed with a field of view covering the head to mid-thigh using a setting of 3 min per bed position for five to eight bed positions. Images were reconstructed using the ordered subsets expectation maximisation algorithm with a reconstructed slice thickness of 3.27 mm and pixel size of 4.7 mm. A CT was acquired for attenuation correction and anatomic localisation at 140 kVp and Smart mA (15–100) without administration of oral or intravenous contrast agent.

### 2.3. <sup>18</sup>FDG PET/MRI acquisition

<sup>18</sup>FDG PET/MRI examinations were performed on a same-site integrated PET/MRI system (Siemens Biograph mMR, Erlangen, Germany), capable of simultaneous PET and MR imaging in one examination. This was performed immediately after the PET/CT using residual tracer activity. PET/MRI was acquired from the skull base to mid-thigh (total of 4–5 bed positions, 4 min per bed position). For each bed position a 2-point Dixon volume-interpolated breath-hold examination (VIBE) sequence was applied to derive an attenuation map (*u*-map) based on 4 tissue types: air, lungs, soft-tissue and fat. Other sequences per bed position included: axial T1 Dixon, axial T2 HASTE and axial free breathing diffusion-weighted imaging (DWI) sequences (*b* values: 50 and 900 s/mm<sup>2</sup>). In addition, axial T1 Dixon sequences were acquired post administration of 0.1 mmol/kg of intravenous gadolinium (Gadobutrol, Bayer Healthcare, Leverkusen, Germany). Detailed PET/MRI sequence parameters are displayed in Table 1.

### 2.4. Qualitative image analysis

Qualitative PET/MRI image analysis was performed independently by two fellowship trained thoracic radiologists (DJM, SMM) using PET/MRI specific viewing software (SyngoVia, Siemens Healthineers, Erlangen, Germany). The two readers, blinded to the PET/CT findings, independently assigned a TNM stage for each patient according the 7<sup>th</sup> edition of the MPM TNM staging system. The individual PET/MRI staging results for the two readers were then compared directly. As integrated PET/MRI is a novel imaging modality, scans with disagreement in TNM staging were discussed and a consensus PET/MRI staging result reached. The consensus PET/MRI staging results were then compared with the final pathological TNM stage. By means of an imaging comparison, TNM staging was also blindly performed on the clinical FDG PET/CTs by a PET fellowship trained thoracic radiologist (DJM)-this was performed separate to the PET/MRI staging, at least 2 weeks apart.

### 2.5. Quantitative image analysis

Measurements of tumour metabolic activity was performed by measuring the maximum standardised uptake value (SUV<sub>max</sub>) on the

attenuation corrected PET/MRI and PET/CT images. Quantitative image analysis was performed on both the PET/MRI and PET/CT scans at a single sitting by a single reader (DJM), at a separate time point to the qualitative staging analysis. Mean apparent diffusion coefficient (ADC) values were measured at the corresponding sites by manually drawing a region of interest (ROI) on the ADC map, derived from the DWI sequence. These measurements were repeated in sample areas of macroscopic talc in subjects where talc was visualised on the non-contrast CT component of the PET/CT examination.

### 2.6. Surgical technique

All patients included in the study underwent a surgical biopsy, and either talc pleurodesis or indwelling percutaneous catheter placement if a trapped lung was present. For subjects deemed surgically resectable, a pleurectomy decortication was performed according to the technique described by Rusch et al. [13]. No subject had an extrapleural pneumonectomy performed. Lymph node sampling and biopsy of the diaphragm and/or pericardium were performed to increase the accuracy of pathological staging at the time of surgery. Diaphragmatic and /or pericardial resection and reconstruction was performed if directly involved by tumour. Six patients (60%) had undergone talc pleurodesis prior to macroscopic pleural resection.

### 2.7. Statistical analysis

Continuous variables are presented as mean  $\pm$  standard deviation (SD). Categorical variables are presented as frequencies and percentages. Inter-observer agreement for PET/MRI TNM staging was assessed by the weighted kappa method. Pearson correlation coefficients were calculated to examine the relationship between  $SUV_{max}$  and  $ADC_{mean}$  values for areas of tumour, and for areas of talc deposition. Students independent *t*-test was used for comparison of continuous variables. Statistical analysis was performed using GraphPad statistical software (GraphPad Software, La Jolla, CA, USA).

## 3. Results

### 3.1. Patients

Amongst the ten included patients, nine had epithelioid-type tumours, and one had a biphasic mesothelioma tumour. The average administered dose of  $^{18}F$ -FDG was  $319.8 \pm 10.8$  MBq (range 307–345 MBq). The average time period between FDG injection and commencement of the clinical PET/CT scan was  $69 \pm 1$  min (range 59–91 minutes), with an average time delay between radiotracer administration (incorporating the clinical PET/CT scan) and commencement of the PET/MRI examination of  $124 \pm 13$  min (range 111–158 minutes). All subjects underwent pleurectomy/decortication. One subject had transmural diaphragmatic invasion on pre-operative imaging, and underwent neo-adjuvant chemotherapy between imaging and pleurectomy/decortication-this subject is excluded from the comparison between imaging and pathological staging. The mean time between imaging and surgery for the remaining patients was 14 days (range 3–26 days).

### 3.2. PET/MRI, PET/CT & pathological staging

The complete PET/MRI, PET/CT and pathological staging information for all 10 subjects is presented in Table 2. In the nine patients that underwent surgery directly following imaging, the overall tumour stage was concordant between PET/MRI and pathological staging in 6 (67%) of cases, and discordant in 3 (33%). This is superior to the staging results for PET/CT, which was concordant with pathological staging in 3 (33%) cases, and discordant in 6 (67%) cases. PET/MRI performed better in T staging than PET/CT, and was concordant with

pathologic T stage in 7 (78%) cases versus 3 (33%) for PET/CT. PET/MRI and PET/CT were equivalent in N staging, both were concordant with pathological N stage in 7 (78%) of cases. For all 10 subjects imaged, overall tumour staging was concordant between PET/MRI and PET/CT in 7 (70%) of cases, and T stage was concordant in 5 (50%) subjects (Figs. 1 & 2). There was good inter-observer agreement for overall PET/MRI tumour stage (weighted kappa 0.63) with moderate inter-reader agreement for T stage (weighted kappa 0.59) and N stage (weighted kappa 0.52). No subject had evidence of metastatic disease on either imaging or pathology.

### 3.3. Quantitative measurements

The mean PET/MRI derived MPM  $SUV_{max}$  was  $5.8 \pm 2.7$  (range 3.6–12.8), with corresponding  $ADC_{mean}$  values of  $1.02 \pm 0.27 \times 10^{-3}$   $mm^2/s$  (range 0.48–1.50  $10^{-3}$   $mm^2/s$ ). We did not find a significant correlation between tumour  $SUV_{max}$  and  $ADC_{mean}$ , with a *r* value of 0.15 (*p* = 0.7).

Six subjects (60%) had evidence of previous talc pleurodesis on the CT component of their FDG PET/CT scans, with corresponding intense FDG uptake. These areas of talc accumulation showed relatively increased metabolic activity compared to areas without visible talc in these 6 subjects, although this did not achieve statistical significance (mean talc  $SUV_{max}$   $7.4 \pm 2.1$  versus mean tumour  $SUV_{max}$   $4.9 \pm 1.7$ , *p* = 0.06). We observed areas of mismatch between FDG uptake on PET and diffusion restriction on DWI in areas of talc accumulation in each subject that had evidence of prior talc pleurodesis on CT (Figs. 3 & 4). These foci of visible talc accumulation had significantly higher mean ADC values compared to areas of metabolically active tumour ( $1.78 \pm 0.47 \times 10^{-3}$   $mm^2/s$  versus  $0.98 \pm 0.34 \times 10^{-3}$   $mm^2/s$ , *p* = 0.007), and we found a moderate positive correlation between talc  $SUV_{max}$  and  $ADC_{mean}$  with a *r* value of 0.75, although this did not reach statistical significance (*p* = 0.08).

## 4. Discussion

In our series, FDG PET/MRI performed well in the loco-regional staging of MPM in comparison to pathological staging. PET/MRI performed better than PET/CT in T staging, which is often the principal deciding factor of whether a patient is eligible for surgical resection [13]. Martini et al. found sequential, co-registered FDG PET + MRI had a comparable diagnostic accuracy compared to FDG PET/CT in 34 patients with MPM, 26 with histopathological confirmation [14]. Integrated FDG PET/MRI has previously been shown to be comparable to FDG PET/CT in MPM staging [12], and our study is the first to compare clinical staging by integrated PET/MRI with gold standard pathological staging.

It is unsurprising that FDG PET/MRI was superior to FDG PET/CT in local tumour staging given the superior soft tissue resolution of MRI compared to CT, particularly the non-contrast CT component of the PET/CT, which is primarily used for attenuation correction and anatomical localisation. Diagnostic quality CT with IV iodinated contrast is the main workhorse for MPM clinical staging, but is subject to poor inter-observer variation, and tends to underestimate pathological stage in up to 58% of patients [15,8,16]. Accurately identifying transdiaphragmatic, transpericardial and chest wall invasion is challenging on CT, even with the use of multi-planar reformats [17]. MRI has been shown to be superior to CT in the identification of occult chest wall, transdiaphragmatic, endothoracic fascial and bone invasion [18–20]. The use of gadolinium contrast and fat suppression allow accurate identification of tumour, helping to distinguish it from pleural fluid and adjacent lung, and to identify subtle invasion into the endothoracic fascia, chest wall or through the diaphragm, increasing the T stage. Diffusion weighted imaging has been shown to be useful in distinguishing between benign pleural plaques and malignant pleural mesothelioma [21], and in the assessment of histological subtypes [22].

**Table 2**  
Summary of clinical and pathological staging.

| Gender              | Age             | Histopathological subtype | TNM stage PET/MRI     | TNM Stage PET/CT      | TNM Stage pathological | PET/MRI stage  | PET/CT stage   | Pathological stage |
|---------------------|-----------------|---------------------------|-----------------------|-----------------------|------------------------|----------------|----------------|--------------------|
| Male                | 71              | Epithelioid               | T3 N0 M0              | T3 N0 M0              | T3 N0 M0               | 3              | 3              | 3                  |
| Male                | 72              | Epithelioid               | T3 N2 M0              | T3 N2 M0              | T3 N0 M0               | 3              | 3              | 3                  |
| Male                | 66              | Biphasic                  | T3 N0 M0              | T3 N0 M0              | T3 N0 M0               | 3              | 3              | 3                  |
| Female <sup>†</sup> | 71 <sup>†</sup> | Epithelioid <sup>†</sup>  | T4 N2 M0 <sup>†</sup> | T4 N2 M0 <sup>†</sup> | T1a N0 M0 <sup>†</sup> | 4 <sup>†</sup> | 4 <sup>†</sup> | 1a <sup>†</sup>    |
| Male                | 68              | Epithelioid               | T3 N0 M0              | T2 N0 M0              | T3 N0 M0               | 3              | 2              | 3                  |
| Male                | 51              | Epithelioid               | T3 N1 M0              | T3 N0 M0              | T1b N0 M0              | 3              | 3              | 1b                 |
| Male                | 69              | Epithelioid               | T2 N2 M0              | T3 N2 M0              | T2 N0 M0               | 3              | 3              | 2                  |
| Male                | 71              | Epithelioid               | T3 N2 M0              | T1b N0 M0             | T3 N2 M0               | 3              | 1b             | 3                  |
| Male                | 73              | Epithelioid               | T2 N0 M0              | T2 N0 M0              | T1b N0 M0              | 2              | 2              | 1b                 |
| Male                | 66              | Epithelioid               | T3 N0 M0              | T2 N0 M0              | T3 N0 M0               | 3              | 2              | 3                  |

PET = positron emission tomography; MRI = magnetic resonance imaging; CT = computed tomography.  
TNM = tumour, nodes and metastasis AJCC malignant pleural mesothelioma staging system, 7th edition.  
<sup>†</sup> underwent neo-adjuvant chemotherapy between imaging and surgery.

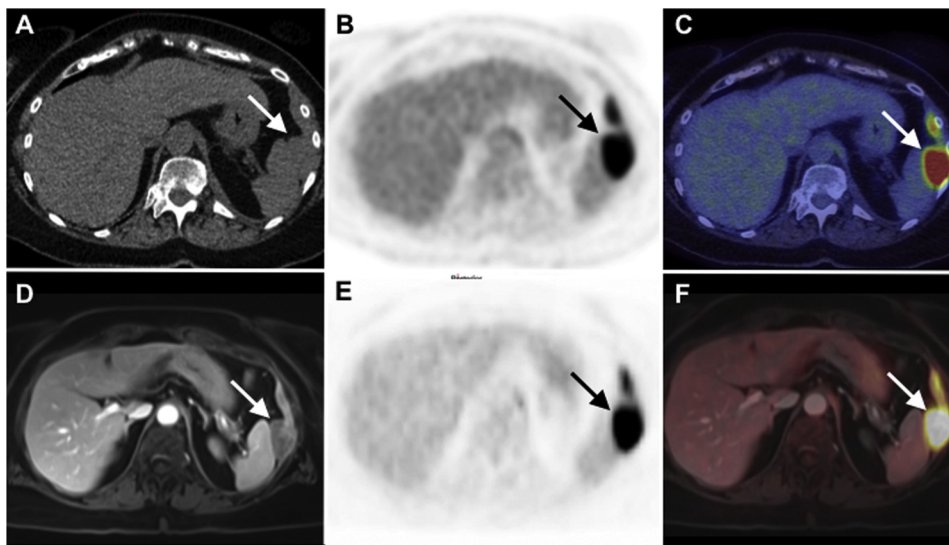


**Fig. 1.** Axial CT (A), PET only (B) and fused FDG PET/CT (C) images in a 71 year old woman with epithelioid malignant pleural mesothelioma shows a metabolically active left basal pleural mass (arrows) with transdiaphragmatic invasion abutting the spleen, consistent with a T4 tumour. Corresponding axial T1 Dixon water sequence post-gadolinium (D), PET only (E) and fused PET/MRI (F) images in the same patient shows similar appearance of the T4 tumour (arrows) with transdiaphragmatic invasion.

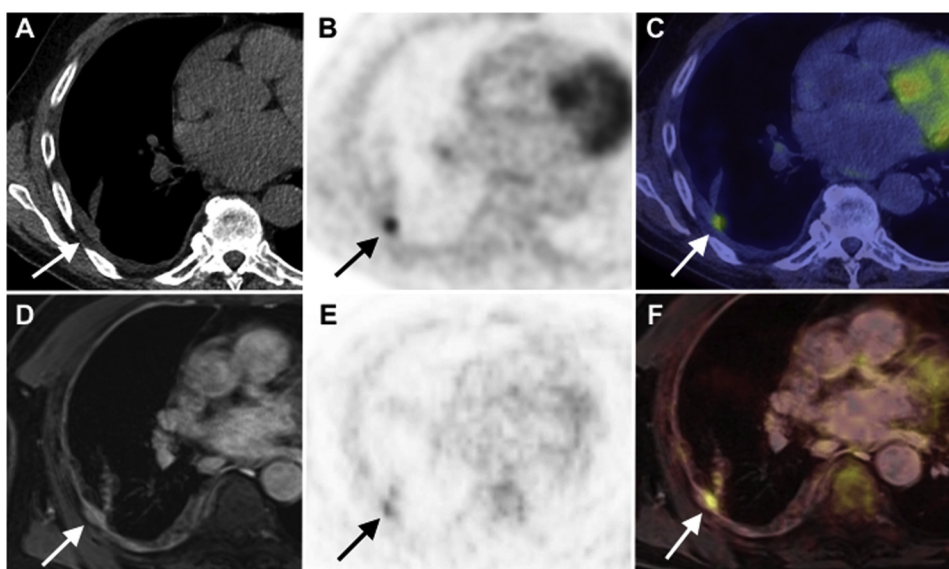


**Fig. 2.** Axial CT (A), PET only (B) and fused FDG PET/CT (C) images in a 68 year old man with epithelioid malignant pleural mesothelioma demonstrates a metabolically active pleural nodule (arrows) in the right posterior hemithorax, staged as a T2 tumour on PET/CT. Corresponding axial T1 post-gadolinium Dixon water (D), PET only (E) and fused PET/MRI (F) images in the same patient show better delineation of the tumour (arrows), particularly on image (D), with local extension into the endothoracic fascia upstaging the patient to a T3 tumour, confirmed at surgery.

The presence of increased FDG uptake on PET has been proven to be useful in distinguishing between benign and malignant pleural disease [23], and FDG PET is excellent at detecting occult metastasis [11]. Tumour SUV<sub>max</sub> has been proposed as a potential prognostic marker [9], and it may also be useful in assessing treatment response [24,25].

The combination of FDG PET and MRI in a single examination has the potential to provide a comprehensive, complete assessment of local and distant tumour staging in a single examination, giving the treating medical and surgical oncology teams the best possible staging information to devise the appropriate personalised treatment plan for the

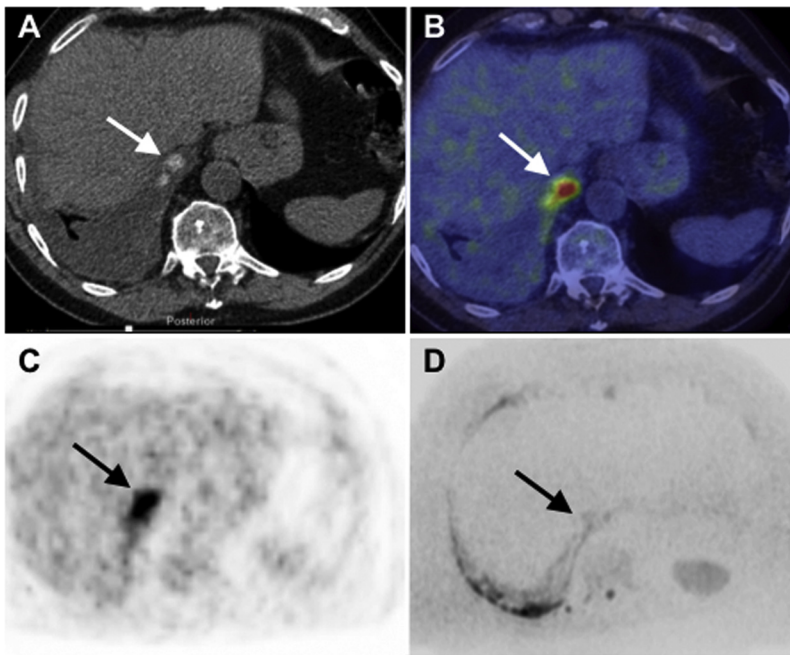


**Fig. 3.** Axial CT (A) and fused FDG PET/CT (B) images in a patient with malignant pleural mesothelioma shows intense tracer uptake at a nodular focus of high attenuation talc accumulation (arrows) in the right medial basal hemithorax. Axial PET only image (C) from a PET/MRI study in the same patient shows corresponding intense tracer uptake in the same location (arrow), but without evidence of restricted diffusion seen on an inverted b900 DWI image (D, arrow) in the same location.

individual patient.

One known disadvantage of FDG PET in MPM staging is in the presence of talc pleurodesis, where a local inflammatory reaction to the presence of talc can result in spurious increased FDG uptake [26]. Our observation of apparent areas of mismatch between FDG uptake and diffusion restriction in areas of talc deposition may be a novel way to discriminate between talc and tumour related FDG uptake; this is still only an observation however, and merits further investigation in a larger cohort to see if it is a clinically useful sign. We did not find an inverse correlation between  $SUV_{max}$  and ADC values in areas of tumour, as was previously demonstrated elsewhere [12]. This may be due to the small number of subjects in our cohort, and difficulties in measuring ADC values in linear areas of malignant pleural thickening due to partial volume averaging. Diffusion restriction has previously been shown to be a useful diagnostic and characterisation metric in MPM [21,22], and we observed areas of diffusion restriction with concordant increased FDG uptake in each subject in our cohort.

There are potential pitfalls to using FDG PET/MRI as a single staging examination for MPM. MRI has an inferior spatial resolution to CT, which may reduce the detection of small pleural or pulmonary nodules [27]. Advances in PET/MRI image acquisition may help to overcome these difficulties. The development of new, free breathing ultrashort echo time MRI sequences greatly improves the quality of pulmonary imaging by MRI over traditional dual echo gradient echo imaging, improving the conspicuity of pulmonary and pleural nodules by PET/MRI [28]. The use of respiratory triggered PET and MRI image acquisition could also improve image quality, leading to improved detection of small sites of pleural or pulmonary disease. Respiratory triggered MRI sequences have traditionally been limited by longer imaging acquisition times, but novel sequences such as the free-breathing respiratory gated T2 weighted PROPELLAR sequence, acquired in approximately 5 min, provides pulmonary imaging free from breathing artefact, with improved nodule detection compared to T1 weighted Dixon sequences [29,30]. The increased slice thickness of PET/MRI

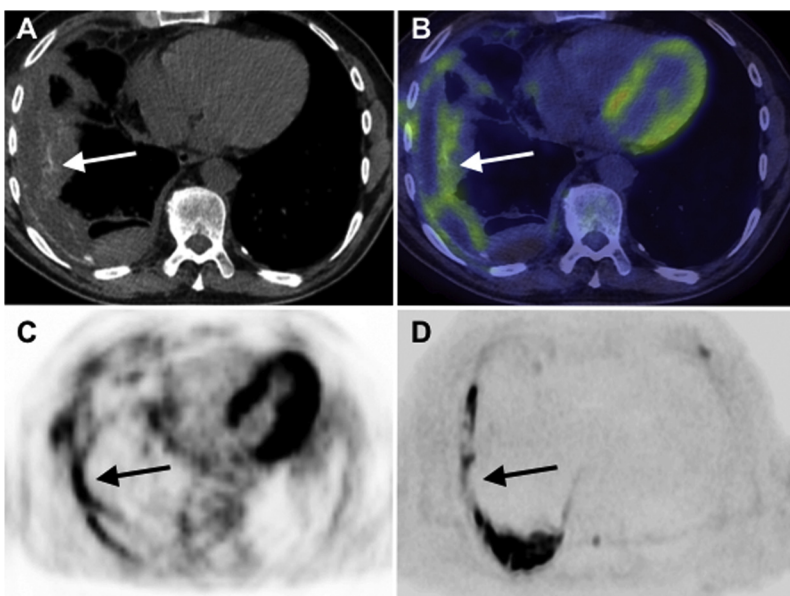


**Fig. 4.** Axial CT (A) and fused FDG PET/CT (B) images in a patient with malignant pleural mesothelioma shows increased FDG uptake at a linear focus of high density talc accumulation (arrows) in the right lateral basal hemithorax. Axial PET only image (C) from a PET/MRI study in the same patient shows corresponding elevated FDG uptake (arrow), with a lack of diffusion restriction in the same region on an inverted b900 DWI image (D, arrow).

compared to PET/CT (typically 4 mm for PET/MRI versus 2.5 mm for PET/CT) may lead to missed lesions due to partial volume averaging, but despite these potential difficulties, we did not find any significant missed lesions by FDG PET/MRI, in line with other similar series [12,14]. Other potential disadvantages to using PET/MRI include the use of gadolinium contrast agents, the length of examination (approximately 60 min with our protocol), and the large cost and lack of current availability of this new modality. Patients with MPM tend to be older and often have breathing difficulties due to pleural disease and other pulmonary comorbidities; it is therefore important to try and reduce examination time by rationalising the number of MRI sequences used where possible, and by using free breathing sequences [31]. Despite the potential complications of gadolinium, we believe that post-contrast imaging is beneficial in MPM staging by PET/MRI, as the fat-saturated post contrast MRI images provides superior delineation of local tumour invasion compared to CT, particularly in the differentiation of tumour from adjacent fluid, atelectasis and fat [20]. Difficulties in performing qualitative staging, and the lack of a quantitative component, have led to questions about the consistency and prognostic accuracy of the current TNM staging system [32,33], with tumour volume potentially a more accurate staging and prognostic metric [15,34,35]. MPM tumour volume measurement performed on post-contrast imaging has been shown to be feasible and reproducible by MRI in the setting of assessing treatment response [36], with better accuracy than CT [37]. The accuracy of tumour volume measurements by MRI could be improved by the addition of a map of tumour metabolic activity provided by the PET component of an FDG PET/MRI scan. FDG PET also allows derivation of the total glycolytic volume (TGV), a combined measure of tumour volume and metabolic activity [38]. TGV appears to be prognostic based on FDG PET/CT studies [10,25,39], and if proven to be feasible with FDG PET/MRI, could provide additional prognostic information beyond TNM staging, and provide a reproducible imaging biomarker for the assessment of metabolic treatment response in clinical trials. The acquisition of dynamic-contrast enhanced (DCE) MRI is another potential benefit of administering gadolinium, and appears promising tool for both MPM diagnosis [40] and disease response assessment [41]. PET/MRI is a promising new modality, which has the potential to provide a comprehensive anatomical and functional examination in a single test.

Our study has limitations. This was a single site study with a small sample size; PET/MRI is a new test and MPM is a relatively rare disease, which made patient recruitment challenging. The CT component of the PET/CT scan was acquired without iodinated IV contrast as per our routine clinical departmental protocol. This does represent a potential source of bias in comparison of the two integrated imaging modalities, but it does represent standard, real-world clinical practice. We did not examine the inter-observer agreement for MPM staging by FDG PET/CT, as this has been previously performed elsewhere [14]. We performed staging according to the 7<sup>th</sup> edition of AJCC TNM staging manual to ensure uniformity across our cohort, as this is what was in operation when our study began in 2015. The 8<sup>th</sup> edition of the MPM TNM is now in clinical practice, however this is unlikely to influence our results significantly, as the differences between the two iterations are small, and do not alter the assessment of tumour resectability [4–6]. We acquired axial MRI images only, and both readers felt that coronal and sagittal acquisitions would be useful to aid tumour staging, particularly when looking for transdiaphragmatic invasion.

In conclusion, our findings suggest that integrated FDG PET/MRI appears feasible for loco-regional staging of MPM, and may be superior to FDG PET/CT, particularly in determining the T stage. In patients who have undergone previous talc pleurodesis, the identification of areas of DWI-FDG mismatch may help to distinguish talc-related pleural FDG uptake from metabolically active tumour, although this observation requires further investigation in a larger cohort to determine its validity.

## Funding source

The authors acknowledge financial support from the Transforming Outcomes and Health Economics through Imaging project funded by Guys and St Thomas' Charity, the King's College London/University College London Comprehensive Cancer Imaging Centres funded by Cancer Research UK and Engineering and Physical Sciences Research Council in association with the Medical Research Council and the Department of Health (C1519/A16463) and the Wellcome Trust EPSRC Centre for Medical Engineering at King's College London (WT203148/Z/16/Z).

## Conflicts

We have no conflicts of interest to declare.

## References

- [1] L.T. Nickell Jr, J.P. Lichtenberger III, L. Khorashadi, G.F. Abbott, B.W. Carter, Multimodality imaging for characterization, classification, and staging of malignant pleural mesothelioma, *Radiographics* 34 (2014) 1692–1706, <https://doi.org/10.1148/rg.346130089>.
- [2] J. Ai, J.P. Stevenson, Current issues in malignant pleural mesothelioma evaluation and management, *Oncologist* 19 (2014) 975–984, <https://doi.org/10.1634/theoncologist.2014-0122>.
- [3] D.J. Murphy, R.R. Gill, Overview of treatment related complications in malignant pleural mesothelioma, *Ann. Transl. Med.* 5 (2017), <https://doi.org/10.21037/atm.2017.03.97> 235–235.
- [4] A.K. Nowak, K. Chansky, D.C. Rice, H.I. Pass, H.L. Kindler, L. Shemanski, et al., The IASLC Mesothelioma Staging Project: proposals for revisions of the T descriptors in the forthcoming eighth edition of the TNM classification for pleural mesothelioma, *J. Thorac. Oncol.* 12 (2016) 2089–2099, <https://doi.org/10.1016/j.jtho.2016.08.147>.
- [5] D. Rice, K. Chansky, A. Nowak, H. Pass, H. Kindler, L. Shemanski, et al., The IASLC mesothelioma staging project: proposals for revisions of the N descriptors in the forthcoming eighth edition of the TNM classification for pleural mesothelioma, *J. Thorac. Oncol.* 12 (2016) 2100–2111, <https://doi.org/10.1016/j.jtho.2016.09.121>.
- [6] V.W. Rusch, K. Chansky, H.L. Kindler, A.K. Nowak, H.I. Pass, D.C. Rice, et al., The IASLC Mesothelioma Staging Project: proposals for the M descriptors and for revision of the TNM stage groupings in the forthcoming (eighth) edition of the TNM classification for mesothelioma, *J. Thorac. Oncol.* 12 (2016) 2112–2119, <https://doi.org/10.1016/j.jtho.2016.09.124>.
- [7] R.R. Gill, V.H. Gerbaudo, D.J. Sugarbaker, H. Hatabu, Current trends in radiologic management of malignant pleural mesothelioma, *Semin. Thorac. Cardiovasc. Surg.* 21 (2009) 111–120, <https://doi.org/10.1053/j.semtcvs.2009.06.011>.
- [8] R.R. Gill, D.P. Naidich, A. Mitchell, M. Ginsberg, J. Erasmus, S.G. Armato, et al., North American multicenter volumetric CT study for clinical staging of malignant pleural mesothelioma: feasibility and logistics of setting up a quantitative imaging study, *J. Thorac. Oncol.* 11 (2016) 1335–1344, <https://doi.org/10.1016/j.jtho.2016.04.027>.
- [9] V.H. Gerbaudo, S. Britz-Cunningham, D.J. Sugarbaker, S.T. Treves, Metabolic significance of the pattern, intensity and kinetics of 18F-FDG uptake in malignant pleural mesothelioma, *Thorax* 58 (2003) 1077–1082, <https://doi.org/10.1136/thorax.58.12.1077>.
- [10] A.K. Nowak, R.J. Francis, M.J. Phillips, M.J. Millward, A.A. van der Schaaf, J. Boucek, et al., A novel prognostic model for malignant mesothelioma incorporating quantitative FDG-PET imaging with clinical parameters, *Clin. Cancer Res.* 16 (2010) 2409–2417, <https://doi.org/10.1158/1078-0432.CCR-09-2313>.
- [11] V.H. Gerbaudo, S.I. Katz, A.K. Nowak, R.J. Francis, Multimodality imaging review of malignant pleural mesothelioma diagnosis and staging, *PET Clin.* 6 (2011) 275–297, <https://doi.org/10.1016/j.cpet.2011.04.001>.
- [12] B.M. Schaarschmidt, L.M. Sawicki, B. Gomez, J. Grueneisen, M. Hoiczky, P. Heusch, et al., Malignant pleural mesothelioma: initial experience in integrated (18)F-FDG PET/MR imaging, *Clin. Imaging* 40 (2016) 956–960, <https://doi.org/10.1016/j.clinimag.2016.05.001>.
- [13] A.S. Wolf, R.M. Flores, Current treatment of mesothelioma: extrapleural pneumectomy versus pleurectomy/decortication, *Thorac. Surg. Clin.* 26 (2016) 359–375, <https://doi.org/10.1016/j.thorsurg.2016.04.003>.
- [14] K. Martini, A. Meier, I. Opitz, W. Weder, P. Veit-Haibach, R.A. Stahel, et al., Diagnostic accuracy of sequential co-registered PET + MR in comparison to PET/CT in local thoracic staging of malignant pleural mesothelioma, *Lung Cancer* 94 (2016) 40–45, <https://doi.org/10.1016/j.lungcan.2016.01.017>.
- [15] R.R. Gill, B.Y. Yeap, R. Bueno, W.G. Richards, Quantitative clinical staging for patients with malignant pleural mesothelioma, *J. Natl. Cancer Inst.* 110 (2017) 1–7, <https://doi.org/10.1093/jnci/djx175>.
- [16] V.W. Rusch, D. Giroux, C. Kennedy, E. Ruffini, A.K. Cangir, D. Rice, et al., Initial analysis of the international association for the study of lung cancer mesothelioma database, *J. Thorac. Oncol.* 7 (2012) 1631–1639, <https://doi.org/10.1097/JTO.0b013e31826915f1>.
- [17] M.T. Truong, C. Viswanathan, M.B.C. Godoy, B.W. Carter, E.M. Marom, Malignant

- pleural mesothelioma: role of CT, MRI, and PET/CT in staging evaluation and treatment considerations, *Semin. Roentgenol.* 48 (2013) 323–334, <https://doi.org/10.1053/j.ro.2013.03.017>.
- [18] R.T. Heelan, V.W. Rusch, C.B. Begg, D.M. Panicek, J.F. Caravelli, C. Eisen, Staging of malignant pleural mesothelioma: comparison of CT and MR imaging, *AJR Am. J. Roentgenol.* 172 (1999) 1039–1047, <https://doi.org/10.2214/ajr.172.4.10587144>.
- [19] Z.J. Wang, G.P. Reddy, M.B. Gotway, C.B. Higgins, D.M. Jablons, M. Ramaswamy, et al., Malignant pleural mesothelioma: evaluation with CT, MR imaging, and PET, *Radiographics* 24 (2004) 105–119, <https://doi.org/10.1148/rg.241035058>.
- [20] M. Yamamuro, V.H. Gerbaudo, R.R. Gill, F.L. Jacobson, D.J. Sugarbaker, H. Hatabu, Morphologic and functional imaging of malignant pleural mesothelioma, *Eur. J. Radiol.* 64 (2007) 356–366, <https://doi.org/10.1016/j.ejrad.2007.08.010>.
- [21] J. Coolen, F. De Keyzer, P. Nafteux, W. De Wever, C. Dooms, J. Vansteenkiste, et al., Malignant pleural mesothelioma: visual assessment by using pleural pointillism at diffusion-weighted MR imaging, *Radiology* 274 (2015) 576–584, <https://doi.org/10.1148/radiol.14132111>.
- [22] R.R. Gill, S. Umeoka, H. Mamata, T.R. Tillemann, P. Stanwell, R. Woodhams, et al., Diffusion-weighted MRI of malignant pleural mesothelioma: preliminary assessment of apparent diffusion coefficient in histologic subtypes, *Am. J. Roentgenol.* 195 (2010) W125–30, <https://doi.org/10.2214/AJR.09.3519>.
- [23] H. Yildirim, M. Metintas, E. Entok, G. Ak, I. Ak, E. Dundar, et al., Clinical value of fluorodeoxyglucose-positron emission tomography/computed tomography in differentiation of malignant mesothelioma from asbestos-related benign pleural disease: an observational pilot study, *J. Thorac. Oncol.* 4 (2009) 1480–1484, <https://doi.org/10.1097/JTO.0b013e3181c0a7ff>.
- [24] A.K. Nowak, R.J. Francis, S.I. Katz, V.H. Gerbaudo, A multimodality imaging review of malignant pleural mesothelioma response assessment, *PET Clin.* 6 (2011) 299–311, <https://doi.org/10.1016/j.cpet.2011.04.002>.
- [25] H.Y. Lee, S.H. Hyun, K.S. Lee, B.-T. Kim, J. Kim, Y.M. Shim, et al., Volume-based parameter of 18F-FDG PET/CT in malignant pleural mesothelioma: prediction of therapeutic response and prognostic implications, *Ann. Surg. Oncol.* 17 (2010) 2787–2794, <https://doi.org/10.1245/s10434-010-1107-z>.
- [26] J.J. Erasmus, M.T. Truong, W.R. Smythe, R.F. Munden, E.M. Marom, D.C. Rice, et al., Integrated computed tomography-positron emission tomography in patients with potentially resectable malignant pleural mesothelioma: staging implications, *J. Thorac. Cardiovasc. Surg.* 129 (2005) 1364–1370, <https://doi.org/10.1016/j.jtcvs.2004.10.034>.
- [27] L.M. Sawicki, J. Grueneisen, C. Buchbender, B.M. Schaarschmidt, B. Gomez, V. Ruhlmann, et al., Comparative performance of <sup>18</sup>F-FDG PET/MRI and <sup>18</sup>F-FDG PET/CT in detection and characterization of pulmonary lesions in 121 oncologic patients, *J. Nucl. Med.* 57 (2016) 582–586, <https://doi.org/10.2967/jnumed.115.167486>.
- [28] N.S. Burris, K.M. Johnson, P.E.Z. Larson, M.D. Hope, S.K. Nagle, S.C. Behr, et al., Detection of small pulmonary nodules with ultrashort echo time sequences in oncology patients by using a PET/MR system, *Radiology* 278 (2016) 239–246, <https://doi.org/10.1148/radiol.2015150489>.
- [29] F. de Galiza Barbosa, J.H. Geismar, G. Delso, M. Messerli, M. Huellner, P. Stolzmann, et al., Pulmonary nodule detection in oncological patients - Value of respiratory-triggered, periodically rotated overlapping parallel T2-weighted imaging evaluated with PET/CT-MR, *Eur. J. Radiol.* 98 (2018) 165–170, <https://doi.org/10.1016/j.ejrad.2017.11.010>.
- [30] T. Küstner, M. Schwartz, P. Martirosian, S. Gatidis, F. Seith, C. Gilliam, et al., MR-based respiratory and cardiac motion correction for PET imaging, *Med. Image Anal.* 42 (2017) 129–144, <https://doi.org/10.1016/j.media.2017.08.002>.
- [31] D.A. Torigian, H. Zaidi, T.C. Kwee, B. Saboury, J.K. Udupa, Z.-H. Cho, et al., PET/MR imaging: technical aspects and potential clinical applications, *Radiology* 267 (2013) 26–44, <https://doi.org/10.1148/radiol.13121038>.
- [32] V.W. Rusch, D. Giroux, Do we need a revised staging system for malignant pleural mesothelioma? Analysis of the IASLC database, *Ann. Cardiothorac. Surg.* 1 (2012) 438–448, <https://doi.org/10.3978/j.issn.2225-319X.2012.11.10>.
- [33] D.A. Waller, The staging of malignant pleural mesothelioma: are we any nearer to squaring the circle? *Eur. J. Cardiothorac. Surg.* 49 (2016) 1648–1649, <https://doi.org/10.1093/ejcts/evz436>.
- [34] D.J. Murphy, R.R. Gill, Volumetric assessment in malignant pleural mesothelioma, *Ann. Transl. Med.* 5 (2017), <https://doi.org/10.21037/atm.2017.05.23> 241–241.
- [35] V.W. Rusch, R. Gill, A. Mitchell, D. Naidich, D.C. Rice, H.I. Pass, et al., A multicenter study of volumetric computed tomography for staging malignant pleural mesothelioma, *Ann. Thorac. Surg.* 102 (2016) 1059–1066, <https://doi.org/10.1016/j.athoracsur.2016.06.069>.
- [36] C. Plathow, M. Klopp, C. Thieke, F. Herth, A. Thomas, A. Schmaehl, et al., Therapy response in malignant pleural mesothelioma-role of MRI using RECIST, modified RECIST and volumetric approaches in comparison with CT, *Eur. Radiol.* 18 (2008) 1635–1643, <https://doi.org/10.1007/s00330-008-0918-9>.
- [37] R. Gill, D. Murphy, R. Seethamraju, R. Bueno, W. Richards, MA 19.10 comparative value of MR and CT for tumor volumetric and clinical staging of malignant pleural mesothelioma, *J. Thorac. Oncol.* 12 (2017) S1886, <https://doi.org/10.1016/j.jtho.2017.09.641>.
- [38] J.A. Boucek, R.J. Francis, C.G. Jones, N. Khan, B.A. Turlach, A.J. Green, Assessment of tumour response with (18)F-fluorodeoxyglucose positron emission tomography using three-dimensional measures compared to SUVmax—a phantom study, *Phys. Med. Biol.* 53 (2008) 4213–4230, <https://doi.org/10.1088/0031-9155/53/16/001>.
- [39] A. Klabatsa, S. Chicklore, S.F. Barrington, V. Goh, L. Lang-Lazdunski, G.J.R. Cook, The association of 18F-FDG PET/CT parameters with survival in malignant pleural mesothelioma, *Eur. J. Nucl. Med. Mol. Imaging* 41 (2014) 276–282, <https://doi.org/10.1007/s00259-013-2561-1>.
- [40] J. Coolen, F. De Keyzer, P. Nafteux, W. De Wever, C. Dooms, J. Vansteenkiste, et al., Malignant pleural disease: diagnosis by using diffusion-weighted and dynamic contrast-enhanced MR imaging—initial experience, *Radiology* 263 (2012) 884–892, <https://doi.org/10.1148/radiol.12110872>.
- [41] M.V. Tomšič, S. Bisdas, V. Kovac, I. Sersa, K.Š. Popovič, Dynamic contrast-enhanced MRI of malignant pleural mesothelioma: a comparative study of pharmacokinetic models and correlation with mRECIST criteria, *Cancer Imaging* (2019) 1–11, <https://doi.org/10.1186/s40644-019-0189-5>.